accepted for publication in *Physical Review E* 2003

Universal finite-size scaling behavior and universal dynamical scaling behavior of absorbing phase transitions with a conserved field

S. Lübeck
Weizmann Institute of Science, Department of Physics of Complex Systems, 76100 Rehovot, Israel,

P. C. Heger
Institut für Theoretische Physik, Universität Duisburg-Essen, 47048 Duisburg, Germany
(Dated: July 13, 2003)

We analyze numerically three different models exhibiting an absorbing phase transition. We focus on the finite-size scaling as well as the dynamical scaling behavior. An accurate determination of several critical exponents allows to validate certain hyperscaling relations. Using this hyperscaling relations it is possible to express the avalanche exponents of a self-organized critical system in terms of the ordinary exponents of a continuous absorbing phase transition.

PACS numbers: 05.70.Ln, 05.50.+q, 05.65.+b

arXiv:cond-mat/0309165v1 [cond-mat.stat-mech] 6 Sep 2003

I. INTRODUCTION

Absorbing phase transition (APT) are a particular class of non-equilibrium phase transitions occurring in physical, biological, as well as chemical systems (see for instance [1]). Transitions to absorbing states are of particular interest since they have no equilibrium counterparts and may occur even in one-dimensional systems. A characteristic feature of absorbing phase transitions is the competition between the proliferation and annihilation of a certain entity A, e.g., particles, energy units, viruses, molecules in catalytic reactions, etc. It is essential that no spontaneous creation of such quantities takes place. At a critical value of the proliferation-annihilation rate the density $\rho(A)$ vanishes and the system is trapped forever in the absorbing state $\rho(A) = 0$.

Directed percolation is recognized as a paradigmatic example of absorbing phase transitions. This is reflected by the universality hypothesis of Janssen and Grassberger that models which exhibit a continuous phase transition to a single absorbing state generally belong to the universality class of directed percolation [2, 3]. Different universality classes occur for instance in the presence of additional symmetries. In particular, particle conservation may lead to the different universality class of absorbing phase transitions with a conserved field as pointed out in [4]. For instance the conserved lattice gas (CLG) [4], the conserved threshold transfer process (CTTP) [4], the well known Manna sandpile model [5], as well as a reaction-diffusion model [6] belong to this universality class [7]. Note that this universality class is of particular interest since the corresponding systems connect the critical behavior of the absorbing phase transition with the critical steady state of self-organized critical (SOC) systems [8]. Actually, SOC sandpile models can be considered as driven-dissipative versions of (closed) systems exhibiting absorbing phase transitions [9].

In this paper we consider the universal finite-size scaling as well as the universal dynamical scaling behavior of the CLG model, the CTTP, and the Manna model. First we introduce a method that allows to study finite-size effects in the steady state. In contrast to previous attempts to measure finite-size effects our method is well defined. Furthermore it can be applied immediately to other classes of absorbing phase transitions. Second we consider the activity spreading of a single active seed. The corresponding spreading exponents are naturally connected to the avalanche exponents of SOC systems [10]. In particular we discuss certain hyperscaling laws relating the spreading exponents to the steady state exponents of absorbing phase transitions. This allows us to express the SOC avalanche exponents in terms of the exponents of the corresponding absorbing phase transition (e.g. the exponents of the order parameter, the correlation length exponent, etc.). Thus the critical state of SOC systems is closely related to the critical properties of an ordinary second order phase transition.

II. MODELS

The first considered model is the conserved lattice gas (CLG) [4] which is a stochastic variant of a model introduced by Jensen [11]. In the CLG model lattice sites may be empty or occupied by one particle. In order to mimic a repulsive interaction a given particle is considered as active if at least one of its neighboring sites on the lattice is occupied by another particle. If all neighboring sites are empty the particle remains inactive. Active particles are moved in the next update step to one of their empty nearest neighbor sites, selected at random.

The second model is the so-called conserved threshold transfer process (CTTP) [4], a modification of the threshold transfer process introduced in [12]. Here, lattice sites may be empty, occupied by one particle, or occupied by two particles. Empty and singly occupied sites are considered as inactive whereas double occupied lattice sites are considered as active. In the latter case one tries to transfer both particles of a given active site to randomly chosen empty or singly occupied nearest neighbor sites.

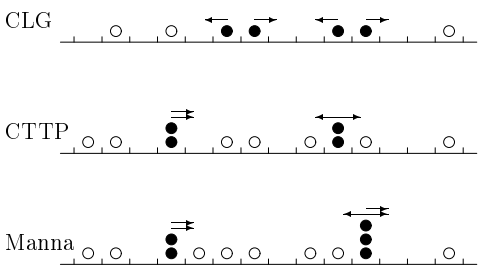

FIG. 1: Sketch of the dynamics of the three considered models. Filled circles mark active particles whereas non-active particles are marked by open circles. The arrows denote how the active particles are (probably) moved in the next update step. In the case of the one-dimensional CLG model the particle transfer is deterministic. For the one-dimensional CTTP stochastic (left) as well as deterministic (right) particle movements may occur. Only the one-dimensional Manna model is characterized by a full stochastic dynamics in $D = 1$.

The third model is a modified version of the Manna sandpile model [5] the so-called fixed-energy Manna model [9]. In contrast to the CTTP the Manna model allows unlimited particle occupation of lattice sites. We use in our investigations the original Manna relaxation rules, i.e., lattice sites which are occupied by at least two particles are considered as active and all particles are moved to the neighboring sites selected at random.

The three models are sketched in Fig. 1. We use in all cases periodic boundary conditions, i.e., closed systems are considered and the number of particles is conserved. In our simulations (see [13, 14] for details) we start from a random distribution of particles. All models reach after a transient regime a steady state which is characterized by the average density of active sites ρ_a. The density ρ_a is the order parameter and the particle density ρ is the control parameter of the absorbing phase transition, i.e., the order parameter vanishes at the critical density ρ_c according to $\rho_a \propto \delta\rho^\beta$, with the reduced control parameter $\delta\rho = \rho/\rho_c - 1$. Additionally to the order parameter we consider its fluctuations $\Delta\rho_a$. Approaching the transition point from above ($\delta\rho > 0$) the fluctuations diverge according to $\Delta\rho_a \propto \delta\rho^{-\gamma'}$ (see [13, 14]). Below the critical density (in the absorbing state) the order parameter as well as its fluctuations are zero in the steady state.

Similar to equilibrium phase transitions it is possible in the case of absorbing phase transitions to apply an external field h which is conjugated to the order parameter, i.e., the field causes a spontaneous creation of active particles (see for instance [1]). A realization of the external field for absorbing phase transitions with a conserved field was developed in [13] where the external field triggers movements of inactive particles which may be activated in this way. At the critical density ρ_c the order parameter and its fluctuations scale as $\rho_a \propto h^{\beta/\sigma}$ and $\Delta\rho_a \propto h^{-\gamma'/\sigma}$, respectively.

It was shown recently that the order parameter and its fluctuations obey in the steady state the scaling forms [7]

$$\rho_a(\delta\rho, h) \sim \lambda^{-\beta}\, \tilde{R}(a_\rho \delta\rho\, \lambda, a_h h\, \lambda^\sigma)\,, \quad (1)$$

$$a_\Delta\, \Delta\rho_a(\delta\rho, h) \sim \lambda^{\gamma'}\, \tilde{D}(a_\rho \delta\rho\, \lambda, a_h h\, \lambda^\sigma)\,. \quad (2)$$

The universal scaling functions $\tilde{R}(x, y)$ and $\tilde{D}(x, y)$ are the same for all systems belonging to a given universality class whereas all non-universal system-dependent features (e.g. the lattice structure, the update scheme, etc.) are contained in the so-called non-universal metric factors a_ρ, a_h, and a_Δ [15]. The universal scaling functions are normed by the conditions $\tilde{R}(1, 0) = \tilde{R}(0, 1) = \tilde{D}(0, 1) = 1$ and the non-universal metric factors can be determined from the amplitudes of

$$\rho_a(\delta\rho, h = 0) \sim (a_\rho\, \delta\rho)^\beta\,, \quad (3)$$

$$\rho_a(\delta\rho = 0, h) \sim (a_h\, h)^{\beta/\sigma}\,, \quad (4)$$

$$a_\Delta\, \Delta\rho_a(\delta\rho = 0, h) \sim (a_h\, h)^{-\gamma'/\sigma}\,. \quad (5)$$

These equations are obtained by choosing in the scaling forms [Eqs. (1, 2)] $a_\rho \delta\rho\, \lambda = 1$ and $a_h h\, \lambda^\sigma = 1$, respectively.

A recently performed analysis of the universal scaling functions as well as of the critical exponents for $D \geq 2$ [7] confirms the conjecture of [4] that the CLG model, the

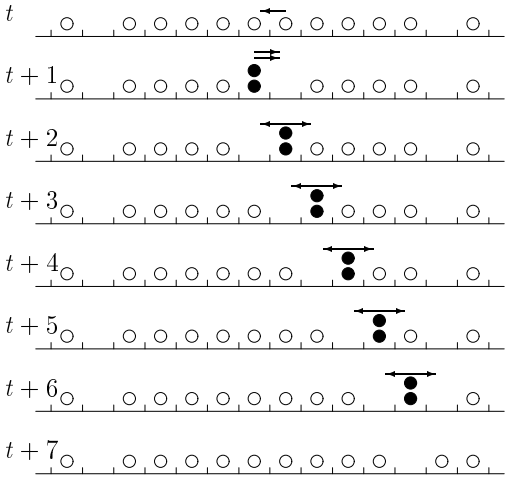

FIG. 2: Sketch of the dynamics of the one-dimensional CTTP. At update step t an active site is triggered by the external field in a cluster of inactive sites. The arrows denote how the active particles (full circles) are moved in the next update step. Due to the dynamic rules of the CTTP only two different relaxation processes (selected randomly) occur: both particles are moved to the same empty site or both particles are moved to two adjacent sites. Thus the dynamics of the one-dimensional CTTP is characterized by a trivial random walk of the perturbation. This random walk proceeds until it reaches the boundary of a cluster.

CTTP, and the Manna model belong to the same universality class. The situation is more complicated in one-dimensional systems where a splitting of the universality class occur. The reason for the non-universal behavior is that the dimensional reduction changes the stochastic character of the dynamics (see Fig. 1.). For instance the CLG model is characterized by deterministic toppling rules in $D = 1$ and exhibits a trivial phase transition with $\beta = 1$ and $\rho_c = 1/2$ (see also ref. 22 in [4]). Due to the trivial behavior of the one-dimensional CLG model we consider in this work the two- and three-dimensional CLG model only.

In the case of the CTTP we observe that roughly 40% of the relaxation events are deterministic. Furthermore a perturbation that is triggered by the external field performs a simple random walk (see Fig. 2). This pathologic behavior is completely different from the behavior of the one-dimensional Manna model that is characterized by a pure stochastic relaxation of active particles to the next neighbors. More than the other models the Manna model is therefore the paradigm of the universality class of absorbing phase transitions with a conserved field. In the following we will call that class the Manna universality class since universality classes are often labeled by the simplest model belonging to them.

The universality splitting of the one-dimensional systems is in full agreement with the universality hypothesis of sandpile models [16]. According to this conjecture the universality classes of sandpile models are determined by the way the particles are distributed to the next neighbors (deterministic, stochastic, directed, undirected, etc.). Obviously the Manna universality class is characterized by a stochastic and undirected distribution of particles.

III. STEADY-STATE FINITE-SIZE SCALING

Similar to equilibrium critical phenomena we assume that the system size L enters the scaling forms [Eqs. (1,2)] as an additional scaling field, i.e.

$$\begin{aligned} \rho_a(\delta\rho, h, L) &\sim \lambda^{-\beta}\tilde{R}_{\rm pbc}(a_\rho\delta\rho\lambda, a_h h\lambda^\sigma, a_L L\lambda^{-\nu_\perp}), \\ a_\Delta\Delta\rho_a(\delta\rho, h, L) &\sim \lambda^{\gamma'}\tilde{D}_{\rm pbc}(a_\rho\delta\rho\lambda, a_h h\lambda^\sigma, a_L L\lambda^{-\nu_\perp}) \end{aligned} \quad (6)$$

where the exponent $\nu_\perp$ describes the divergence of the spatial correlation length, i.e., $\xi_\perp \propto \delta\rho^{-\nu_\perp}$. Note that the universal scaling functions depend now on the particular choice of the boundary conditions, the system shape etc. [15]. Throughout this work we use in all dimensions hyper cubic lattices with periodic boundary conditions (pbc). However, the universal scaling functions [Eqs. (1,2)] are recovered in the thermodynamic limit, e.g.

$$\tilde{R}_{\rm pbc}(x, y, \infty) = \tilde{R}(x, y). \quad (7)$$

Additionally to the order parameter and its fluctuations we consider the fourth-order cumulant Q which is defined as (see for instance [17])

$$Q = 1 - \frac{\langle\rho_a^4\rangle}{3\langle\rho_a^2\rangle^2}. \quad (8)$$

For non-vanishing order-parameter the cumulant tends to $Q = 2/3$ in the thermodynamic limit. In the case of a zero order parameter the cumulant vanishes if the order parameter is characterized by a Gaussian distribution symmetrically distributed around zero. The latter case is observed in equilibrium systems, e.g. the Ising model for $T > T_c$. In the case of absorbing phase transitions the order parameter is non-negative per definition. Thus the order parameter is characterized by a non-trivial distribution close to criticality and the above scenario does not apply.

Nevertheless one expects that the cumulant obeys the scaling form

$$Q(\delta\rho, h, L) \sim \tilde{Q}_{\rm pbc}(a_\rho\delta\rho\,\lambda, a_h h\,\lambda^\sigma, a_L L\,\lambda^{-\nu_\perp}). \quad (9)$$

Notice that no metric factor a_Q is needed since the cumulant is already dimensionless. Choosing $a_L L\,\lambda^{-\nu_\perp} = 1$ we get for zero-field

$$\begin{aligned} Q(0,0,L) &= Q(\delta\rho, 0, L)\Big|_{\delta\rho=0} \\ &\sim \tilde{Q}_{\rm pbc}(a_\rho\delta\rho\,(a_L L)^{-\nu_\perp}, 0, 1)\Big|_{\delta\rho=0} \\ &= \tilde{Q}_{\rm pbc}(0,0,1) \end{aligned} \quad (10)$$

which is obviously universal. The universal value $\tilde{Q}_{\rm pbc}(0,0,1)$ corresponds to an intersection point if one plots Q as a function of ρ for various system sizes L. Thus it is possible to determine the critical value ρ_c from the common intersection point. This cumulant intersection method is very useful and was applied in numerous works (see for instance [17] and references therein).

As usually finite-size effects have to be taken into account if the correlation length is of the order of the system size. A feature of these finite-size effects is that a given system may pass within the simulations from one phase to the other. This behavior is caused by critical fluctuations, i.e., approaching the transition point the order parameter vanishes whereas its fluctuations diverge. But in contrast to common second order phase transitions the situation is drastically different in the case of absorbing phase transitions. Approaching the transition point the correlation length $\xi_\perp$ increases and as soon as $\xi_\perp$ is of the order of L the system may pass to an absorbing state and is trapped forever. Additionally to the absorbing phase ($\langle\rho_a^k\rangle = 0$ for $\delta\rho < 0$) the steady state order parameter and its higher moments vanish ($\langle\rho_a^k\rangle_L = 0$) even in a small vicinity above the critical point. Thus in the case of absorbing phase transitions it is impossible to consider finite-size effects of steady state quantities around the critical point.

In order to bypass this problem it was suggested (see for instance [18]) to consider metastable (ms) or quasi-steady state values of the order parameter and its higher

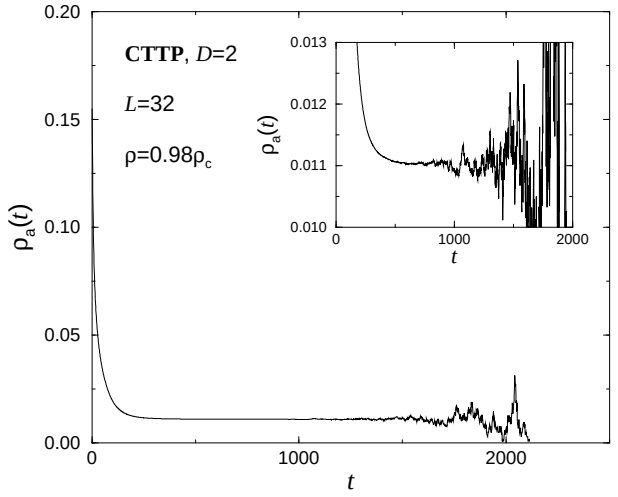

FIG. 3: The decay of the order parameter close to criticality for the two-dimensional CTTP. After a so-called metastable regime the system passes to the absorbing phase. The inset displays that no clear saturation of the order parameter could be observed.

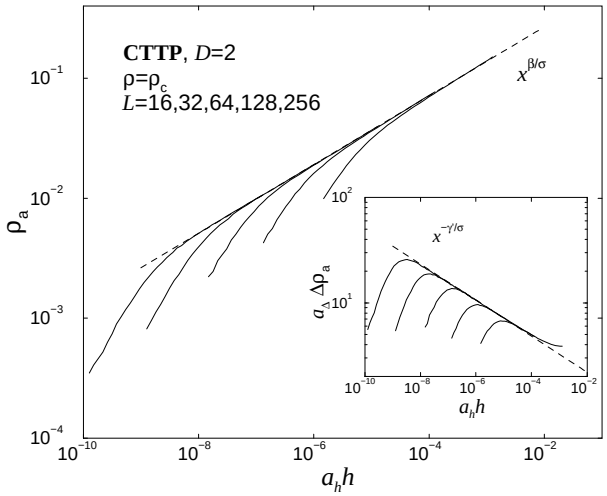

FIG. 4: The density of active sites $\rho_{\rm a}$ as a function of the external field for various system sizes L. The inset displays the corresponding order parameter fluctuations. The dashed-lines correspond to the asymptotic behavior of the infinite systems [Eqs.(4, 5)].

moments $\langle \rho_{\rm a}^k \rangle_{L,\rm ms}$, respectively. This is shown in Fig. 3 for the order parameter of the two-dimensional CTTP close to the transition point. After a short transient regime the system reaches a metastable state where it can spend a certain time until it finally enters an absorbing state. In the metastable phase the order parameter is expected to fluctuate around a well defined average value $\langle \rho_{\rm a} \rangle_{L,\rm ms}$ which is used for the finite-size scaling analysis. This method was applied in previous works (e.g. [4, 9, 18] and the results sound mostly valid.

Nevertheless this method can be questioned. First, there is no well defined average value of the order parameter in the metastable regime. This can be seen in the inset of Fig. 3 where we scrutinize the data. No clear saturation of the order parameter can be observed. Second the method is quite inefficient. In the case of the data presented in Fig. 3 we used $5\,10^7$ different initial configurations for $L = 32$ to get a sufficiently averaged estimate of the order parameter. Although roughly 10^{11} lattice updates ($t_{\rm max} \approx 2000$) were performed no clear saturation could be observed. Thus reliable data for larger lattice sizes ($L = 64, 128, 256, ...$), which are required for an appropriate finite-size scaling analysis, can not be obtained within moderate computer times. Third and finally no rigorous prove exists that the metastable order parameter moments $\langle \rho_{\rm a}^k \rangle_{L,\rm ms}$ scale in the same way as the corresponding steady state order parameter moments.

In contrast to the consideration of metastable phases we choose a different method in order to study finite-size effects in the steady state. In our simulations we measure the order parameter at the critical density ($\delta\rho = 0$) as a function of the conjugated field h for various system sizes. Due to the external field the system can not be trapped forever in the absorbing phase. Therefore steady state quantities are available for all densities. In Fig. 4 we present the order parameter and its fluctuations for the two-dimensional CTTP model. The finite-size effects, i.e., the deviations from the behavior of the "infinite" system ($L \gg \xi_\perp$) can be clearly seen. Note that the data for $L = 32$ are averaged over $3\,10^7$ lattice updates and we obtain smooth curves of the order parameter, its fluctuations as well as of the cumulant. Thus the numerical effort of this method is significantly smaller than the above discussed analysis of the metastable regime.

According to the above scaling laws [Eqs. (6,9)] the finite-size scaling forms are given by

$$\begin{aligned} \rho_{\rm a}(0,h,L) &\sim (a_L L)^{-\beta/\nu_\perp} \tilde{R}_{\rm pbc}(0, a_h h (a_L L)^{\sigma/\nu_\perp}, 1), \\ a_\Delta \Delta\rho_{\rm a}(0,h,L) &\sim (a_L L)^{\gamma'/\nu_\perp} \tilde{D}_{\rm pbc}(0, a_h h (a_L L)^{\sigma/\nu_\perp}, 1), \\ Q(0,h,L) &\sim \tilde{Q}_{\rm pbc}(0, a_h h (a_L L)^{\sigma/\nu_\perp}, 1). \end{aligned} \tag{11}$$

For the sake of convenience we norm the universal scaling function $\tilde{Q}_{pbc}$ by the condition

$$\tilde{Q}_{\rm pbc}(0,1,1) = 0. \tag{12}$$

Since the metric factor a_h is known from previous simulations [7] (via Eq. (4)) the above condition can be used to determine the metric factor a_L. Taking into account that the correlation length scales at criticality as

$$a_\perp \xi_\perp \sim (a_h\, h)^{-\nu_\perp/\sigma} \tag{13}$$

we find that Eq. (12) implies that the universal function $\tilde{Q}_{pbc}$ is positive for $a_L L > a_\perp \xi_\perp$ and negative for $a_L L < a_\perp \xi_\perp$. Note that in the case of equilibrium phase transitions Eq. (12) is useless since the cumulant is usually positive.

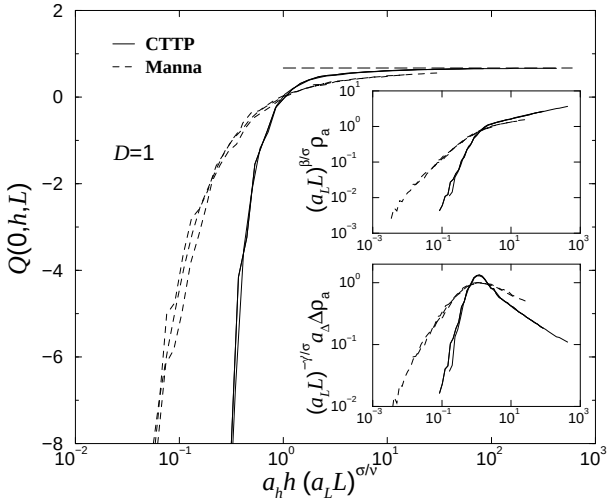

FIG. 5: The universal finite-size scaling analysis of the order parameter ρ_a, of the fluctuations $\Delta\rho_a$ as well as of the cumulant Q for the one dimensional CTTP and the one-dimensional Manna model. The long-dashed lines correspond to the power law behaviors of the infinite system [Eqs.(4, 5)] and to the cumulant limit 2/3, respectively. The data are obtained from simulations of system sizes $L \in \{2048, 4096, 8192\}$ where up to 10^{10} lattice update steps are performed.

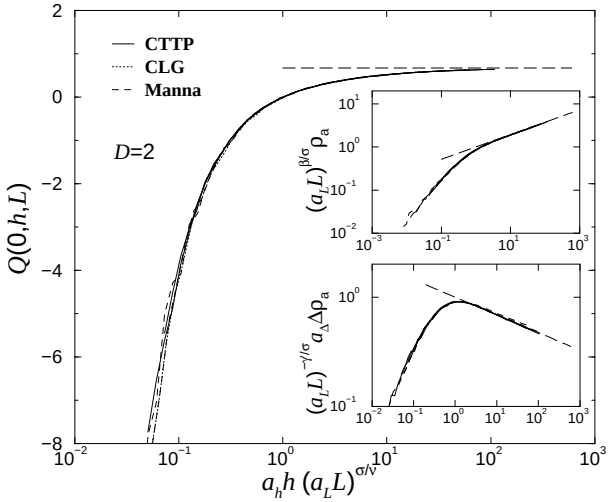

FIG. 6: The universal finite-size scaling analysis of the order parameter ρ_a, of the fluctuations $\Delta\rho_a$ as well as of the cumulant Q for the two dimensional models. The long-dashed lines correspond to the power law behaviors of the infinite system [Eqs.(4, 5)] and to the cumulant limit 2/3, respectively. The data are obtained from simulations of system sizes $L \in \{64, 128, 256\}$ where up to $5\,10^7$ lattice update steps are performed.

In Figs. 5-7 we present the universal finite-size scaling analysis of the CLG model, the Manna model and the CTTP for $D = 1, 2, 3$. Since the exponents β and σ were already determined in previous works [7, 13, 14] we just vary the correlation length exponent $\nu_\perp$ in order to produce data collapses. The value of the non-universal metric factor a_L is determined via Eq. (12). We observe good data collapses for $\nu_\perp = 0.799 \pm 0.014$ for $D = 2$ and $\nu_\perp = 0.593 \pm 0.013$ for $D = 3$, respectively. The data collapses are quite sensitive for variations of the exponents. Thus the quality of the corresponding data collapses are used to estimate the error-bars. The values of the exponents as well as of the non-universal metric factors are listed in Table I and Table II.

In the case of the one dimensional Manna model and the one dimensional CTTP we observe the expected splitting of the universality class. The correlations length exponent $\nu_\perp$, the field exponent σ, as well as the scaling functions differ clearly (see Table I and Fig. 5). Furthermore the value of the Manna model $\nu_\perp = 1.347 \pm 0.091$ differs clearly from $\nu_\perp = 1.80 \pm 0.01$ obtained in a previous work including a finite-size scaling analysis of metastable states [19].

Despite this splitting of universality we observe that the fourth-order cumulant tends for all models in all dimensions to infinity if one approaches the transition point, i.e.,

$$\tilde{Q}_{\rm pbc}(0, x, 1) \;\to\; -\infty \quad \text{for} \quad x \;\to\; 0\,. \qquad (14)$$

This behavior is caused by the vanishing steady state fluctuations [see Eq. (8)]. Thus we assume that the divergent fourth-order cumulant is a characteristic feature of all absorbing phase transitions, independently of the considered lattice structure as well as of the particular considered universality class. Preliminary simulations for directed percolation support this conjecture and will be published elsewhere.

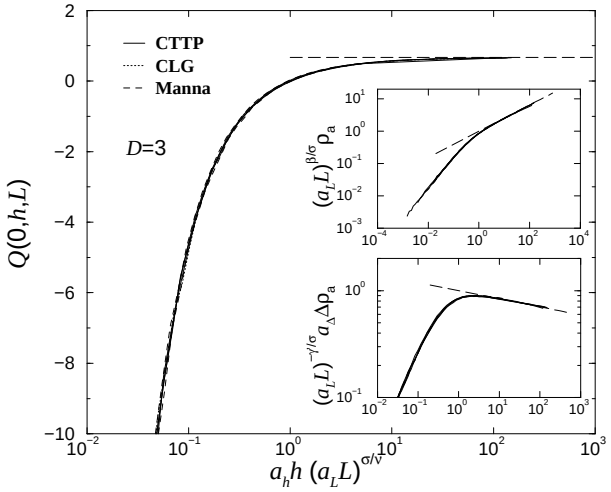

FIG. 7: The universal finite-size scaling analysis of the order parameter ρ_a, of the fluctuations $\Delta\rho_a$ as well as of the cumulant Q for the three dimensional models. The long-dashed lines correspond to the power law behaviors of the infinite system [Eqs.(4, 5)] and to the cumulant limit 2/3, respectively. The data are obtained from simulations of system sizes $L \in \{16, 32, 64\}$ where up to $5\,10^7$ lattice update steps are performed.

IV. DYNAMICAL SCALING BEHAVIOR

A. Homogeneous particle source

In the following we investigate the dynamical scaling behavior in the vicinity of the absorbing phase transition. First we consider how the order parameter $\rho_{\rm a}$ decays, starting the simulations from a random distribution of particles (so-called homogeneous particle source). Above the transition point the density of active sites decreases in time and tends to the steady state value (despite of finite-size effects as discussed above). Below the transition point the density of active sites decreases exponentially to zero. At the critical point the order parameter decays algebraically according to

$$\rho_{\rm a} \;\sim\; (a_t t)^{-\alpha} \tag{15}$$

where a_t denotes a corresponding non-universal metric factor. A finite system size limits this power-law behavior and one expects that the order parameter obeys at criticality the scaling ansatz

$$\rho_{\rm a}(L,t) \;\sim\; \lambda^{-\alpha\nu_\parallel}\; \tilde{R}'_{\rm pbc}(a_t t\,\lambda^{-\nu_\parallel}, a_{\scriptscriptstyle L} L\,\lambda^{-\nu_\perp}) \tag{16}$$

where we have to distinguish the universal functions $\tilde{R}'$ and $\tilde{R}$. For the sake of simplicity we choose $\tilde{R}'(1,\infty)=1$. Setting $a_{\scriptscriptstyle L} L\lambda^{-\nu_\perp}=1$ one gets the finite-size scaling form

$$\rho_{\rm a}(L,t) \;\sim\; L^{-\alpha z}\,\tilde{R}'_{\rm pbc}(a_t t\,(a_{\scriptscriptstyle L} L)^{-z}, 1) \tag{17}$$

where $z=\nu_\parallel/\nu_\perp$ denotes the dynamical exponent as usual. Finite-size effects have to be taken into account for $\mathcal{O}(t)=t_{\rm FSS}$ with

$$t_{\rm FSS} \;=\; a_t^{-1}\,(a_{\scriptscriptstyle L} L)^z\,. \tag{18}$$

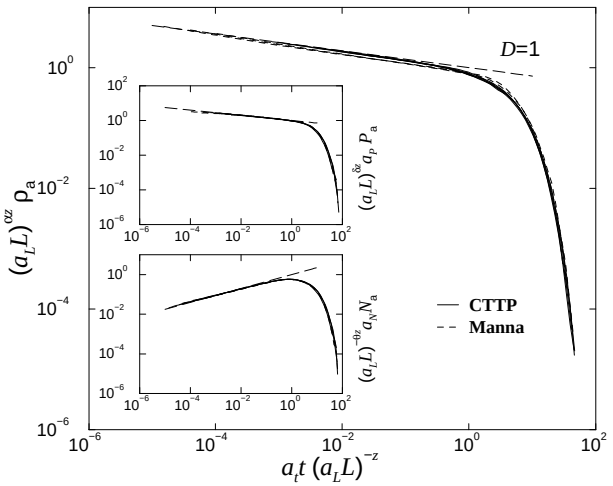

FIG. 8: The dynamical scaling analysis for the one-dimensional CTTP and the Manna model. The long-dashed lines correspond to the power law behaviors of the infinite systems [Eqs. (15, 21, 22)]. System sizes from $L=512$ up to $L=8192$ are considered and the data are averaged over at least 10^5 different initial natural configurations (see text).

For $t \ll t_{\rm FSS}$ the scaling function obeys the power-law $\tilde{R}'_{\rm pbc}(x,1) \sim x^{-\alpha}$, whereas $\tilde{R}'_{\rm pbc}(x,1)$ decays exponentially for $x \gg 1$, i.e., $t \gg t_{\rm FSS}$.

According to the above scaling form [Eq. (17)] we plot in the Figs. 8-10 the rescaled order parameter as a function of the rescaled time. We observe good data collapses for $\alpha = 0.419 \pm 0.015$, $z = 1.533 \pm 0.024$ for $D=2$ and $\alpha = 0.745 \pm 0.017$, $z = 1.823 \pm 0.023$ for $D=3$, respectively. These values are in agreement with

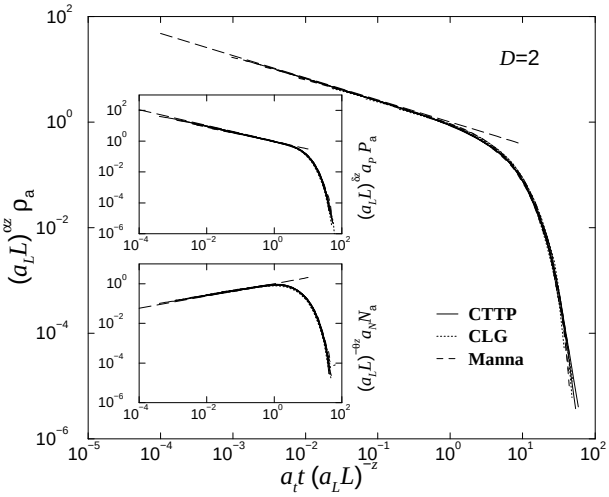

FIG. 9: The dynamical scaling analysis for the two-dimensional models. The long-dashed lines correspond to the power law behaviors of the infinite systems [Eqs. (15, 21, 22)]. System sizes from $L=64$ up to $L=512$ are considered and the data are averaged over at least $2\,10^6$ different initial natural configurations (see text).

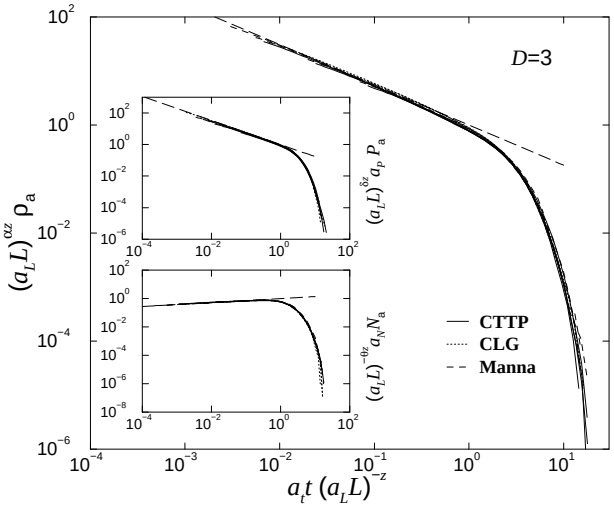

FIG. 10: The dynamical scaling analysis for the three-dimensional models. The long-dashed lines correspond to the power law behaviors of the infinite systems [Eqs. (15, 21, 22)]. System sizes from $L=16$ up to $L=128$ are considered and the data are averaged over at least $5\,10^6$ different initial natural configurations (see text).

those of previous simulations [4]. In the case of the one-dimensional models we observe that the CTTP and the Manna model are both characterized by $\alpha = 0.141 \pm 0.024$ and $z = 1.393 \pm 0.037$ but the corresponding scaling curves of both models differ slightly. It is possible that this indicates a universality splitting similar to the steady state scaling behavior.

B. Localized particle source

Additionally to a homogeneously distributed source of active sites one usually considers the activity spreading generated from a single active seed [20]. In this case it is customary to examine the survival probability $P_{\mathrm{a}}(t)$ that the system is still active after t update steps. Furthermore one investigates how the number of active sites $N_{\mathrm{a}}(t)$ increases in time. At criticality the survival probability as well as the average number of active sites are expected to scale as

$$a_P\, P_{\mathrm{a}}(L,t) \;\sim\; \lambda^{-\delta\nu_\parallel}\, \tilde{P}_{\mathrm{pbc}}(a_t t\, \lambda^{-\nu_\parallel}, a_L L\, \lambda^{-\nu_\perp})\,, \quad (19)$$

$$a_N\, N_{\mathrm{a}}(L,t) \;\sim\; \lambda^{\theta\nu_\parallel}\, \tilde{N}_{\mathrm{pbc}}(a_t t\, \lambda^{-\nu_\parallel}, a_L L\, \lambda^{-\nu_\perp})\,. \quad (20)$$

The universal functions are normed by $\tilde{P}(1,\infty) = 1$ and $\tilde{N}(1,\infty) = 1$ and we find in the thermodynamic limit

$$a_P\, P_{\mathrm{a}} \;\sim\; (a_t t)^{-\delta}\,, \quad (21)$$

$$a_N\, N_{\mathrm{a}} \;\sim\; (a_t t)^{\theta}\,. \quad (22)$$

The finite-size scaling forms are obtained by setting $a_L L \lambda^{-\nu_\perp} = 1$, yielding

$$a_P\, P_{\mathrm{a}}(L,t) \;\sim\; L^{-\delta z}\, \tilde{P}_{\mathrm{pbc}}(a_t t\, (a_L L)^{-z}, 1)\,, \quad (23)$$

$$a_N\, N_{\mathrm{a}}(L,t) \;\sim\; L^{\theta z}\, \tilde{N}_{\mathrm{pbc}}(a_t t\, (a_L L)^{-z}, 1)\,. \quad (24)$$

Again the scaling functions $\tilde{P}_{\mathrm{pbc}}$ and $\tilde{N}_{\mathrm{pbc}}$ decay exponentially for $t \gg t_{\mathrm{FSS}}$ whereas they exhibit an algebraic behavior for $t \ll t_{\mathrm{FSS}}$.

Since the absorbing state is non-trivial one has to investigate the spreading activity at the so-called natural density (see for instance [18]). For each considered model an absorbing state at ρ_{c} is prepared and a particle is moved to a randomly selected site in order to create one active seed. We obtain for all dimensions convincing data collapses which are shown in the insets of the Figs. 8-10. The values of the exponents agrees with those of previous works [4] and are listed together with the non-universal metric factors in Table I and Table II. In summary activity spreading from a localized seed is characterized for all three models by the same universal scaling functions $\tilde{P}$ and $\tilde{N}$.

The activity spreading of APT with a conserved field is closely connected to avalanche processes in SOC systems [9]. In particular the Manna model is a paradigmatic example of a class of SOC systems, the so-called sandpile models. The SOC version and the APT version of the Manna model are characterized by the same

TABLE I: The critical exponents of the considered models below the upper critical dimension $D_{\mathrm{c}} = 4$. The data of the exponents β and σ are obtained from [14]. The finite-size scaling analysis yields the values of $\nu_\perp$ and γ', whereas the exponents α, δ, θ, and z are obtained from activity spreading (see text). The values of β' and $\nu_\perp$ are determined via scaling laws. In particular the values of $\nu_\parallel$ are in good agreement with those of direct measurements of the order parameter persistence distribution [27]. In the case of the one-dimensional models we observe a splitting of the universality class.

	$D=1$	$D=2$	$D=3$
α	0.141 ± 0.024	0.419 ± 0.015	0.745 ± 0.017
δ	0.170 ± 0.025	0.510 ± 0.020	0.765 ± 0.025
θ	0.350 ± 0.030	0.310 ± 0.030	0.140 ± 0.030
z	1.393 ± 0.037	1.533 ± 0.024	1.823 ± 0.023
β	0.382 ± 0.019	0.639 ± 0.009	0.840 ± 0.012
β'	$0.319 \pm 0.052_{\mathrm{Manna}}$	0.624 ± 0.029	0.827 ± 0.034
σ	$2.710 \pm 0.040_{\mathrm{Manna}}$	2.229 ± 0.032	2.069 ± 0.043
	$1.770 \pm 0.058_{\mathrm{CTTP}}$		
$\nu_\perp$	$1.347 \pm 0.091_{\mathrm{Manna}}$	0.799 ± 0.014	0.593 ± 0.013
	$1.760 \pm 0.060_{\mathrm{CTTP}}$		
$\nu_\parallel$	$1.876 \pm 0.135_{\mathrm{Manna}}$	1.225 ± 0.029	1.081 ± 0.027
	$2.452 \pm 0.106_{\mathrm{CTTP}}$		
γ'	$0.550 \pm 0.040_{\mathrm{Manna}}$	0.367 ± 0.019	0.152 ± 0.017
	$0.670 \pm 0.040_{\mathrm{CTTP}}$		

(microscopic) dynamic rules but the boundary conditions differ. Closed boundary conditions lead to a globally conserved particle density in the case of absorbing phase transitions. Whereas sandpile models are per definition driven dissipative systems where particles (sand-grains) are injected into the system and dissipated through open boundaries. The self-organization of SOC systems corresponds to the fact that they approach, without any external fine tuning, the critical state ($\rho(t) \to \rho_{\mathrm{c}}$) in the infinitesimally slow driving limit (so-called separation of time scales, see [21]). In the critical state the external driving triggers (scale invariant) avalanche-like relaxation events. These avalanche processes are described by certain critical exponents which can be derived from the spreading exponents δ, θ, and z [9, 10]. In particular the avalanches are characterized by several quantities (see for instance [16, 22]), e.g. the size s (number of elementary relaxation events), the area a (number of distinct toppled sites), the time t (number of parallel updates until the configuration is stable), as well as the radius exponent r (radius of gyration). In the critical steady state the corresponding probability distributions decay algebraically

$$P_x \;\propto\; x^{-\tau_x}\,, \quad (25)$$

characterized by the avalanche exponents τ_x with $x \in \{s, a, t, r\}$. Assuming that the size, area, etc. scale as a power of each other,

$$x \;\propto\; x'^{\gamma_{xx'}} \quad (26)$$

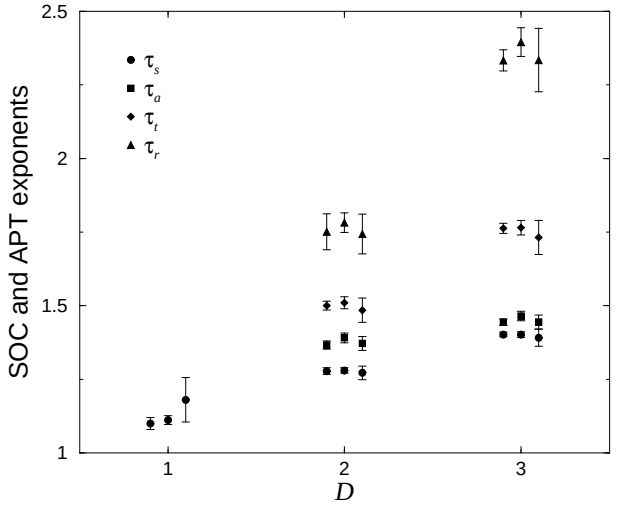

FIG. 11: The avalanche exponents of the Manna model in various dimensions. In order to avoid overlaps the exponents are slightly shifted. The avalanche exponents of the SOC version of the Manna model (left) are obtained from [26] for $D = 1$ and from [23, 25] for $D = 2, 3$. Using the Eqs. (29-33) we obtained the avalanche exponents (middle) from the spreading exponents δ, θ, and z. Using certain hyperscaling relations it is possible to express the avalanche exponents (right) in terms of the exponents of the continuous absorbing phase transition, see Eqs. (54-57).

one obtains the scaling relations

$$\gamma_{xx'} \;=\; \frac{\tau_{x'} - 1}{\tau_x - 1}\,. \tag{27}$$

The exponent γ_{tr} equals the dynamical exponent z, the exponent γ_{ar} corresponds to the fractal dimension of the avalanches and the exponent γ_{sa} indicates whether multiple toppling events are relevant ($\gamma_{sa} > 1$) or irrelevant ($\gamma_{sa} = 1$).

These avalanche exponents are connected to the spreading exponents δ, θ, and z (see for instance [10]). First the survival probability $P_{\rm a}(t)$ is simply given by the integrated avalanche duration

$$P_{\rm a}(t) \;=\; \sum_{t'=t}^{\infty} P_t(t') \tag{28}$$

yielding

$$\tau_t \;=\; 1 \,+\, \delta\,. \tag{29}$$

Since $\gamma_{tr} = z$ the radius exponent is given by

$$\tau_r \;=\; 1 \,+\, z\,\delta\,. \tag{30}$$

Taking into account that the avalanches of the Manna model are compact ($\gamma_{ar} = D$) below the upper critical dimension $D_{\rm c} = 4$ [22, 23] we find

$$\tau_a \;=\; 1 \,+\, \frac{z\,\delta}{D}\,. \tag{31}$$

Finally the number of topplings s_t for an avalanche that is active at time t equals the integrated numbers of active sites, i.e.,

$$s_t\, P_{\rm a}(t) \;=\; \sum_{t'=0}^{t} N_{\rm a}(t') \tag{32}$$

leading to [10]

$$\tau_s \;=\; 1 \,+\, \frac{\delta}{1+\theta+\delta}\,. \tag{33}$$

Thus the avalanche exponents of the Manna model are naturally related to the spreading exponents of the absorbing phase transition. In Fig. 11 we compare our results with those of SOC simulations of the Manna model. The data show that the above scaling relations [Eqs. (29-33)] are fulfilled.

V. DISCUSSION

In this section we check several scaling relations. Due to the pathological behavior of the one-dimensional CTTP we use the corresponding values of the Manna model for our consideration. At the beginning we check the scaling relation

$$\gamma' \;=\; D\,\nu_\perp \,-\, 2\,\beta \tag{34}$$

which can be easily derived from the scaling form of the order parameter histogram (see for instance [18]). The corresponding data are plotted in Fig. 12. As can be seen the above scaling relation is fulfilled within the errorbars.

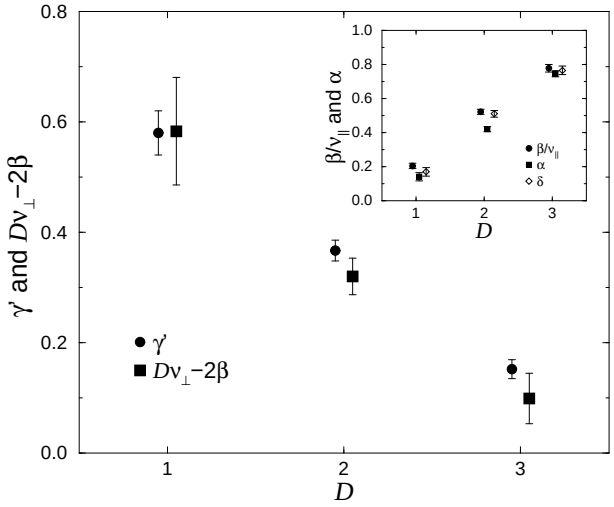

FIG. 12: Test of the scaling relations $\gamma' = D\nu_\perp - 2\beta$, $\alpha = \beta/\nu_\parallel$ (inset), as well as $\delta = \beta/\nu_\parallel$ (inset).

Taking into consideration that a weak external field may trigger spreading events one finds that the field exponent is given by [1]

$$\sigma \;=\; D\,\nu_\perp \,+\, \nu_\parallel \,-\, \nu_\parallel\,\delta\,. \tag{35}$$

In Fig. 13 we check this scaling law. As can be seen it is fulfilled within the error-bars.

Next we consider the hyperscaling relation

$$\theta \;=\; \frac{D}{z} \,-\, \frac{\beta}{\nu_\parallel} \,-\, \delta. \tag{36}$$

This scaling relation can be derived if one assumes that the steady state scaling forms and the dynamical scaling forms can be combined to

$$\begin{aligned} & N_{\rm a}(\delta\rho, h, L, t, \rho_{\rm a,0}) = L^D\;\rho_{\rm a}(\delta\rho, h, L, t, \rho_{\rm a,0}) \\ \sim\;& L^D\,\lambda^{-\beta}\tilde{R}_{\rm pbc}(a_\rho\delta\rho\lambda, a_h h\lambda^\sigma, \\ & a_L L\lambda^{-\nu_\perp}, a_t t\lambda^{-\nu_\parallel}, a_0\rho_{\rm a,0}\lambda^{D\nu_\perp-\nu_\parallel\delta})\,. \end{aligned} \tag{37}$$

Here the initial density of active sites $\rho_{\rm a,0}$ appears as an additional scaling field (see for instance [1] and references therein) and the scaling function behaves asymptotically as

$$\tilde{R}_{\rm pbc}(0,0,\infty,1,x) \;\sim\; \begin{cases} x & \text{for} \quad x \ll 1 \\ \text{const} & \text{for} \quad x \gg 1\,. \end{cases} \tag{38}$$

Starting at criticality from a low density of active sites (e.g. several seeds) the number of active sites increases as $N_{\rm a} \propto t^\theta$ until it reaches a maximum and crosses over to the expected asymptotic decay $\rho_{\rm a} \propto t^{-\alpha}$. The crossover time is determined by

$$\mathcal{O}(a_0\rho_{\rm a,0}\,(a_t t_{\rm co})^{D/z-\delta}) \;=\; 1 \tag{39}$$

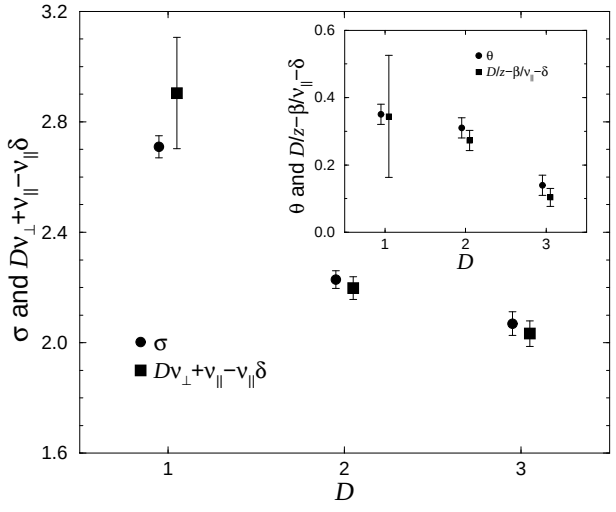

FIG. 13: Test of the hyperscaling relations $\sigma = D\nu_\perp + \nu_\parallel - \nu_\parallel\delta$. and $\theta = D/z - \beta/\nu_\parallel - \delta$ (see inset).

which corresponds to a merging of the survived (and former separated) clusters of activity [1]. The scaling of the crossover time explains the choice of the scaling exponents in Eq. (37). Setting $a_t t\lambda^{-\nu_\parallel} = 1$ we find at criticality

$$\begin{aligned} & N_{\rm a}(0,0,L,t,\rho_{\rm a,0}) \sim L^D\;(a_t t)^{-\beta/\nu_\parallel} \\ & \tilde{R}_{\rm pbc}(0,0,a_L L(a_t t)^{-1/z}, 1, a_0\rho_{\rm a,0}(a_t t)^{D/z-\delta})\,. \end{aligned} \tag{40}$$

The full crossover can be observed if the particular value of the initial density of active sites $\rho_{\rm a,0}$ leads to $1 \ll t_{\rm co} \ll t_{\rm FSS}$ (as it was for instance observed for directed percolation [1]). Therefore, the first regime [Eq. (22)] is obtained for $1 \ll t \ll t_{\rm co}$, the second regime [Eq. (15)] for $t_{\rm co} \ll t \ll t_{\rm FSS}$ and finite-size effects take place in the third regime for $t > t_{\rm FSS}$.

In the case that one starts the simulations with a single seed $\rho_{\rm a,0} = L^{-D}$ we get $t_{\rm co} \propto L^{zD/(D-z\delta)}$. Taking into account that $z < zD/(D-z\delta)$ we find that $t_{\rm FSS} < t_{\rm co}$, i.e., finite size effects take place before the algebraic decay of active particles starts [Eq. (15)] and the second scaling regime does not occur. Furthermore we can use for $t \ll t_{\rm FSS}$ the approximation

$$\begin{aligned} & \tilde{R}_{\rm pbc}(0,0,a_L L(a_t t)^{-1/z}, 1, a_0 L^{-D}(a_t t)^{D/z-\delta}) \\ \approx\;& \tilde{R}_{\rm pbc}(0,0,\infty, 1, a_0\rho_{\rm a,0}(a_t t)^{D/z-\delta}) \\ \sim\;& a_0\,L^{-D}\,(a_t t)^{D/z-\delta} \end{aligned} \tag{41}$$

and Eq. (40) reads now

$$N_{\rm a} \;\sim\; a_0\,(a_t t)^{-\beta/\nu_\parallel + D/z-\delta}\,. \tag{42}$$

Comparing this result with Eq. (22) we obtain the hyperscaling relation Eq. (36) as well as $a_0 = 1/a_N$. In the inset of Fig. 13 we display the data of the corresponding exponents. The hyperscaling relation Eq. (36) is fulfilled within the error-bars.

The situation is completely different if one starts the simulations with a homogeneous particle source. For instance a random distribution of particles leads for the two-dimensional CTTP to an initial density $\rho_{\rm a,0} \approx 0.1703$. In that case the crossover time

$$t_{\rm co} \;=\; \frac{1}{a_t}\left(\frac{1}{a_N}\,\rho_{\rm a,0}\right)^{-\frac{1}{D/z-\delta}} \;\approx\; 1.14 \tag{43}$$

is too small and the short time scaling regime ($N_{\rm a} \propto t^\theta$ for $1 \ll t \ll t_{\rm co}$) can not be observed. On the other hand the scaling form Eq. (37) yields for the second regime ($t_{\rm co} \ll t \ll t_{\rm FSS}$)

$$\begin{aligned} & \rho_{\rm a}(\delta\rho, h, L, t, \rho_{\rm a,0}) \\ \sim\;& (a_t t)^{-\beta/\nu_\parallel}\tilde{R}_{\rm pbc}(0,0,a_L L(a_t t)^{-1/z}, 1, a_0\rho_{\rm a,0}t^{D/z-\delta}) \\ \approx\;& (a_t t)^{-\beta/\nu_\parallel}\tilde{R}_{\rm pbc}(0,0,\infty,1,\infty)\,. \end{aligned} \tag{44}$$

Comparing this result with Eq. (15) we get the scaling relation

$$\alpha \;=\; \frac{\beta}{\nu_\parallel}\,. \tag{45}$$

as well as $\tilde{R}_{\rm pbc}(0,0,\infty,1,\infty) = 1$. But as can be seen from the inset of Fig. 12 this scaling relation is clearly violated in $D = 1$ and $D = 2$. For $D = 3$ we think that the violation of Eq. (45) is hidden by the overlapping error-bars, i.e., the above scaling relation is violated below the upper critical dimension, as already observed in previous simulations [4]. Furthermore the violation of the scaling relation Eq. (45) explains why the well known hyperscaling relation of directed percolation

$$\theta + \alpha + \delta = \frac{D}{z} \tag{46}$$

is not fulfilled for absorbing phase transitions with a conserved field.

It is worth to mention that this scaling anomaly is not caused by the particular initial configuration (random distribution of particles). We have observed the same behavior for a *more* natural initial configuration, where the correlations of the active and non-active sites are not trivial. In this case we start the simulations from a steady state at the critical density with non-zero field h. Switching off the external field we have measured the relaxation of the order parameter from the initial density $\rho_{\rm a,0} = \rho_{\rm a}(\rho_{\rm c}, h)$. For $\rho_{\rm a,0} \approx 0.1$ we observe the same scaling function and the same exponent α as in the case of a random initial configuration.

A possible explanation of the above scaling anomaly is that the asymptotic scaling regime is so far not observed. The situation is sketched in Fig. 14. In the case of the two-dimensional CTTP the crossover takes place at $t_{\rm co} \approx 1.14$ whereas finite-size effects occur at $t_{\rm FSS} \approx 6000$ for $L = 512$. Thus the condition $t_{\rm co} \ll t \ll t_{\rm FSS}$ seems to be fulfilled and one would expect to observe the asymptotic

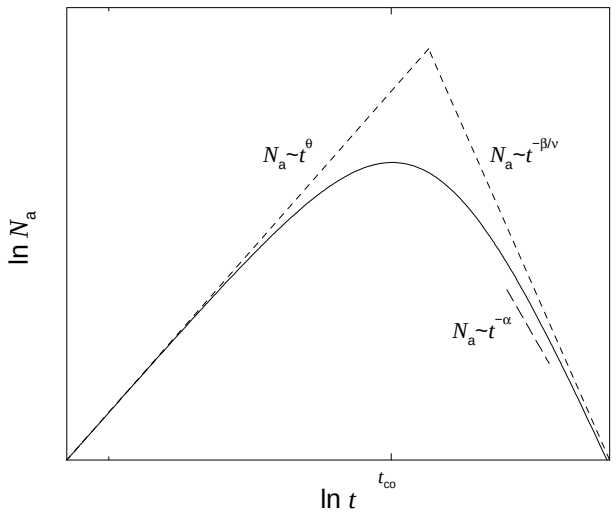

FIG. 14: Sketch of the crossover behavior of the number of active sites $N_{\rm a}$. For $t \ll t_{\rm co}$ $N_{\rm a}$ scales as t^{θ} whereas it is expected to decrease for $t \gg t_{\rm co}$ as $N_{\rm a} \propto t^{-\beta/\nu_\parallel}$. It is possible that a too low exponent ($\alpha < \beta/\nu_\parallel$) is observed in simulations if one has not reached the asymptotic scaling regime (long-dashed line).

scaling behavior $t^{-\beta/\nu_{||}}$. But it is known that crossovers span several decades of magnitudes, usually 5, 6, 7 or even more decades (see for instance [24] for a recent work on crossover effects for the same universality class). In this way it is possible that one observes in simulations a smaller exponent ($\alpha = 0.419$) than the asymptotic value ($\beta/\nu_{||} = 0.522$). Future work on larger lattice sizes ($L \gg 512$) are needed to clarify whether the scaling anomaly can be explained by a simple crossover effect.

Finally we consider the percolation probability $P_{\rm perc}$ that a path of active sites propagates through the system. Obviously the percolation probability is related to the survival probability via

$$P_{\rm perc} = \lim_{t\to\infty} P_{\rm a}(t)\,. \tag{47}$$

The percolation probability is expected to vanish at the critical density according to

$$P_{\rm perc} \propto \delta\rho^{\beta'}\,. \tag{48}$$

Assuming that the survival probability obeys the scaling form

$$\begin{aligned} &a_P\, P_{\rm a}(\delta\rho, L, t) \\ &\sim \lambda^{-\delta\nu_\parallel}\, \tilde{P}_{\rm pbc}(a_\rho\delta\rho\lambda, a_t t\,\lambda^{-\nu_\parallel}, a_L L\lambda^{-\nu_\perp}) \end{aligned} \tag{49}$$

we find in the thermodynamic limit

$$\begin{aligned} P_{\rm perc} &= \lim_{t\to\infty} P_{\rm a}(\delta\rho, t, \infty) \\ &\sim a_P^{-1}\,(a_\rho\delta\rho)^{\delta\nu_\parallel}\,\tilde{P}_{\rm pbc}(1,\infty,\infty) \end{aligned} \tag{50}$$

leading to the scaling relation

$$\delta = \frac{\beta'}{\nu_\parallel}\,. \tag{51}$$

Thus the hyperscaling relations Eq. (35, 36) read now

$$\sigma = \nu_\perp D + \nu_\parallel - \beta'\,, \tag{52}$$

$$\theta = \frac{\nu_\perp D - \beta - \beta'}{\nu_\parallel}\,. \tag{53}$$

In the case of directed percolation β equals β' due to a special symmetry under time reversal [20]. In a more general context one expects that both exponents differ [1], for instance in systems with infinitely many absorbing states or as in our case, in systems where a conserved field couples to the order parameter. The number of independent critical exponents is therefore expected to be four (e.g. β, β', $\nu_\parallel$, $\nu_\perp$) instead of three independent exponents for directed percolation (β, $\nu_\parallel$, $\nu_\perp$). In order to check this scenario we compare in the inset of Fig. 12 the spreading exponent δ with $\beta/\nu_\parallel$. Surprisingly we observe that both values agree within the error-bars for all dimensions, suggesting $\beta = \beta'$. It is possible that the uncertainty of our estimates hides a tiny difference of both exponents. A more accurate test of the scaling relation $\beta = \beta'$ could be obtained by a direct measurement of the percolation probability which remains the topic of future research.

TABLE II: The non-universal metric factors of the considered models. The uncertainty of the metric factors is less than 5%.

	$D=1$	$D=2$	$D=3$
CTTP			
a_ρ	0.607	0.341	0.384
a_h	0.220	0.013	0.093
a_Δ	187.7	45.42	24.51
a_L	1014.	4.617	2.173
a_t	1379.	24.90	4.239
a_P	0.107	0.078	0.094
a_N	6.062	2.818	1.069
CLG			
a_ρ		0.509	0.434
a_h		0.062	0.391
a_Δ		9.241	8.881
a_L		2.107	1.441
a_t		11.22	3.140
a_P		0.157	0.183
a_N		1.249	0.569
Manna			
a_ρ	0.662	0.211	0.311
a_h	$7.52\,10^{-5}$	0.007	0.074
a_Δ	588.9	78.56	32.24
a_L	205.9	6.011	2.367
a_t	$7.99\,10^{4}$	35.53	4.824
a_P	0.063	0.059	0.089
a_N	64.02	3.600	1.229

VI. CONCLUSIONS

We analyzed numerically the critical behavior of three different models exhibiting a continuous phase transition into an absorbing state. In particular we introduce a method which allows to consider finite-size effects in the steady state. It is therefore possible to obtain accurate estimates of the correlation length exponent. Additionally we determine the spreading exponents which describe the spreading of activity at the critical point. A detailed analysis of certain scaling relations shows that usual hyperscaling relations are fulfilled. Only the activity spreading from a homogeneous particle source exhibits a scaling anomaly. So far this scaling anomaly is not understood and remains the topic of future research. The number of independent exponents is due to the scaling anomaly of the exponent α at least four. In the case that $\beta \neq \beta'$ it is even five.

Since the hyperscaling relations Eqs. (35, 36) are fulfilled it is possible to connect the SOC avalanche exponents to the steady state exponents of the corresponding absorbing phase transition:

$$\begin{aligned} \tau_r &= 1 + z + D - \frac{\sigma}{\nu_\perp} \\ &= 1 + \frac{\beta'}{\nu_\perp}, \end{aligned} \tag{54}$$

$$\begin{aligned} \tau_t &= 2 + \frac{D}{z} - \frac{\sigma}{\nu_\parallel} \\ &= 1 + \frac{\beta'}{\nu_\parallel}, \end{aligned} \tag{55}$$

$$\begin{aligned} \tau_a &= 2 + \frac{z}{D} - \frac{\sigma}{D\nu_\perp} \\ &= 1 + \frac{\beta'}{D\nu_\perp}, \end{aligned} \tag{56}$$

$$\begin{aligned} \tau_s &= 1 + \frac{\nu_\parallel + \nu_\perp D - \sigma}{\nu_\parallel + \nu_\perp D - \beta} \\ &= 1 + \frac{\beta'}{\nu_\parallel + \nu_\perp D - \beta}\,. \end{aligned} \tag{57}$$

In Fig. 11 we compare these values with the avalanche exponents obtained from SOC simulations of the Manna model [23, 25, 26]. All SOC exponents agree within the error-bars with the avalanche exponents derived via the above scaling laws. Thus it is possible to express the avalanche exponents (τ_s, τ_a,...) of SOC systems in terms of the usual critical exponents of a second order phase transition (β, $\nu_\perp$, $\nu_\parallel$, ...). In this way, the critical state of SOC sandpile models is closely related to the critical state of an ordinary second order phase transition.

Acknowledgments

We would like to thank A. Hucht, D. Dhar, P. K. Mohanty, and A. Vespignani for helpful discussions and useful comments. P. C. Heger thanks the Weizmann Institute for warm hospitality during a visit when this work was in progress. This work was financially supported by the Minerva Foundation (Max Planck Gesellschaft) as well as by the Deutscher Akademischer Austauschdienst (DAAD).

[1] H. Hinrichsen, Adv. Phys. **49**, 815 (2000).
[2] H. K. Janssen, Z. Phys. B **42**, 151 (1981).
[3] P. Grassberger, Z. Phys. B **47**, 365 (1982).
[4] M. Rossi, R. Pastor-Satorras, and A. Vespignani, Phys. Rev. Lett. **85**, 1803 (2000).
[5] S. S. Manna, J. Phys. A **24**, L363 (1991).
[6] R. Pastor-Satorras and A. Vespignani, Phys. Rev. E **62**, 5875 (2000).
[7] S. Lübeck and P. C. Heger, Phys. Rev. Lett. **90**, 230601 (2003).
[8] P. Bak, C. Tang, and K. Wiesenfeld, Phys. Rev. Lett. **59**, 381 (1987).

[9] A. Vespignani, R. Dickman, M. A. Muñoz, and S. Zapperi, Phys. Rev. E **62**, 4564 (2000).

[10] M. A. Muñoz, R. Dickman, A. Vespignani, and S. Zapperi, Phys. Rev. E **59**, 6175 (1999).

[11] H. J. Jensen, Phys. Rev. Lett. **64**, 3103 (1990).

[12] J. F. F. Mendes, R. Dickman, M. Henkel, and M. C. Marques, J. Phys. A **27**, 3019 (1994).

[13] S. Lübeck, Phys. Rev. E **65**, 046150 (2002).

[14] S. Lübeck, Phys. Rev. E **66**, 046114 (2002).

[15] V. Privman and M. E. Fisher, Phys. Rev. B **30**, 322 (1984).

[16] A. Ben-Hur and O. Biham, Phys. Rev. E **53**, R1317 (1996).

[17] K. Binder and D. W. Heermann, *Monte Carlo Simulation in Statistical Physics* (Springer, Berlin, 1997).

[18] I. Jensen and R. Dickman, Phys. Rev. E **48**, 1710 (1993).

[19] R. Dickman *et al.*, Phys. Rev. E **64**, 056104 (2001).

[20] P. Grassberger and A. de la Torre, Ann. Phys. (N.Y.) **122**, 373 (1979).

[21] G. Grinstein, in *Generic scale invariance and self-organized criticality,* in *Scale Invariance, Interfaces, and Non-Equilibrium Dynamics*, edited by A. McKane *et al.*, NATO ASI Series B: Physics Vol. 344 (Plenum Press, London, 1995).

[22] S. Lübeck and K. D. Usadel, Phys. Rev. E **56**, 5138 (1997).

[23] S. Lübeck, Ph.D. thesis, Gerhard-Mercator-Universität Duisburg, 1998.

[24] S. Lübeck, Phys. Rev. Lett. **90**, 210601 (2003).

[25] S. Lübeck, Phys. Rev. E **61**, 204 (2000).

[26] R. Dickman, M. A. Muñoz, A. Vespignani, and S. Zapperi, Braz. J. Phys. **30**, 27 (2000).

[27] S. Lübeck and A. Misra, Eur. Phys. J. B **26**, 75 (2002).